

# $\Lambda_c^\pm$ production in $pp$ collisions with a new fragmentation function

B. A. Kniehl<sup>1</sup>, G. Kramer<sup>1</sup>, I. Schienbein<sup>2</sup> and H. Spiesberger<sup>3</sup>

<sup>1</sup> II. Institut für Theoretische Physik, Universität Hamburg,  
Luruper Chaussee 149, D-22761 Hamburg, Germany

<sup>2</sup> Laboratoire de Physique Subatomique et de Cosmologie,  
Université Joseph Fourier Grenoble 1,  
CNRS/IN2P3, Institut National Polytechnique de Grenoble,  
53 avenue des Martyrs, F-38026 Grenoble, France

<sup>3</sup> PRISMA<sup>+</sup> Cluster of Excellence, Institut für Physik,  
Johannes-Gutenberg-Universität, Staudinger Weg 7, D-55099 Mainz, Germany

April 10, 2020

## Abstract

We study inclusive  $\Lambda_c^\pm$ -baryon production in  $pp$  collisions in the general-mass variable-flavor number scheme and compare with data from the LHCb, ALICE and CMS collaborations. We perform a new fit of the  $c \rightarrow \Lambda_c^+$  fragmentation function combining  $e^+e^-$  data from OPAL and Belle. The agreement with LHC data is slightly worse compared with a calculation using an older fragmentation function, and the tension between different determinations of  $\Lambda_c^\pm$  production cross sections from the LHC experimental collaborations is not resolved. The ratio of data for  $\Lambda_c^+$ -baryon and  $D^0$ -meson production seems to violate the universality of  $c$ -charm quark to  $c$ -hadron fragmentation.

PACS: 12.38.Bx, 12.39.St, 13.85.Ni, 14.40.Nd

# 1 Introduction

The inclusive production of hadrons containing the heavy charm or bottom quarks,  $c$  and  $b$ , plays an important role in testing quantum chromodynamics (QCD). The predictions in the framework of perturbative QCD are based on the factorization approach. Cross sections are calculated as a convolution of three terms: the parton distribution functions (PDFs) describing the parton content of the initial hadronic state (for a review, see Ref. [1]), the partonic hard-scattering cross sections calculated as perturbative series in powers of the strong-coupling constant, and the fragmentation functions (FFs), which describe the production yield and the momentum distribution for a given heavy-quark hadron originating from a parton. The PDFs and the FFs are non-perturbative objects and determined from experimental data.

Inclusive production of charmed baryons, in particular of  $\Lambda_c^\pm$ , is of interest for several reasons. First, there is the general question whether the perturbative approach to calculate production cross sections applies to  $c$ -baryons in the same way as it does for  $c$ -mesons. The details of the fragmentation mechanism of  $c$ -quarks and other partons, for example gluons, into  $c$ -baryons and into  $c$ -mesons may be different, in particular at small transverse momentum. The new data from the experiments at the LHC are expected to provide us with valuable information to answer this question. Actually, there are indications that, in the case of bottom quarks, universality of the  $\Lambda_b^0$  fragmentation process is violated as discussed in detail in Ref. [2]. It was shown that the  $b \rightarrow \Lambda_b^0$  fragmentation fraction obtained from  $pp$  and  $p\bar{p}$  data is not compatible with that deduced from LEP data. Similar discrepancies might be expected for the case of charmed-baryon production.

So far, FFs for charmed hadrons have been derived from data obtained in  $e^+e^-$  annihilation. These data are well suited for a determination of FFs since they are free from uncertainties due to the properties of the initial state. Very detailed and precise data for charmed-meson and -baryon production, including  $D^0$ ,  $\bar{D}^0$ ,  $D^\pm$ ,  $D^{*\pm}$ ,  $D_s^\pm$ , and  $\Lambda_c^\pm$ , have been obtained by the Belle collaboration at the KEK storage ring [3]. Fragmentation functions for the  $D$  mesons have been obtained from these data combined with earlier LEP data from the OPAL collaboration by T. Kneesch and three of us [4]. A fit of the  $c \rightarrow \Lambda_c^+$  FF was, however, not performed in that work.

A common ansatz for heavy-quark FFs was given by Peterson et al. [5] and is defined by

$$D_c(x, \mu_0) = N \frac{x(1-x)^2}{[(1-x)^2 + \epsilon x]^2}, \quad (1)$$

where  $x$  is the momentum fraction transferred from the charm quark to the observed charm hadron and  $N$  and  $\epsilon$  are parameters fitted to data at an initial scale  $\mu_0$ . The FF is evolved to larger scales  $\mu > \mu_0$  by the DGLAP evolution equations. Two of us have used this ansatz in 2005 and 2006 [6, 7] to obtain the first FFs for  $\Lambda_c^\pm$ . The FFs in these two references differed in the initial condition. The starting scale in Ref. [6] was  $\mu_0 = 2m_c$ , and in Ref. [7]  $\mu_0 = m_c$  was chosen instead, with the charm quark mass  $m_c = 1.5$  GeV. The FFs were obtained from fits to data of the normalized differential cross section  $(1/\sigma_{tot})d\sigma/dx$  for

$e^+e^- \rightarrow \gamma/Z \rightarrow \Lambda_c^\pm$  measured by the OPAL collaboration at LEP1 [8]. The OPAL data include  $b$ -tagged events where the  $\Lambda_c^\pm$  baryons originate from  $b$ -quarks. This contribution was fitted in Ref. [6, 7] with a power ansatz:

$$D_b(x, \mu_0^b) = Nx^\alpha(1-x)^\beta, \quad (2)$$

with  $\mu_0^b = 5$  GeV. The parameter values for  $N$ ,  $\alpha$ ,  $\beta$  and  $\epsilon$  can be found in Refs. [6, 7].

The  $\Lambda_c^\pm$  FFs constructed in Ref. [7] were later used to predict cross sections in the general-mass variable-flavour-number scheme (GM-VFNS) for inclusive  $\Lambda_c^\pm$  production at the LHC, see Ref. [9], where the center-of-mass energy ( $\sqrt{S} = 7$  TeV) is much higher than the energy at which the FFs have been fitted to data ( $\sqrt{S} = M_Z$ ). Corresponding measurements of inclusive  $\Lambda_c^\pm$  production in  $pp$  collisions at LHC energies have been done first by the LHCb collaboration [10]. These measurements are in reasonably good agreement with the previous calculations of Ref. [9] at transverse momenta  $2 < p_T < 8$  GeV and for the rapidity range  $2.0 < y < 4.5$ . The more recent ALICE data for inclusive  $\Lambda_c^\pm$  production at  $\sqrt{S} = 7$  TeV in the central rapidity region  $|y| < 0.5$  [11] have been compared to a calculation with the FFs from Ref. [7] in the range  $3 < p_T < 8$  GeV. In this case, the predictions underestimate the ALICE data [11]: the latter have been found to be larger by a factor of 2.5, on average, than the result of the GM-VFNS calculation at the default choice for factorization and renormalization scales, and outside the theoretical uncertainties obtained from variations of the scale parameters. The most recent measurements of  $d\sigma/dp_T$  for inclusive  $\Lambda_c^\pm$  production are from the CMS collaboration at the LHC [12]. These measurements have been done at  $\sqrt{S} = 5.02$  TeV in the rapidity interval  $|y| < 1.0$  for  $p_T$  between 5 and 20 GeV. We will compare these data with GM-VFNS calculations using the FFs from Ref. [7] below.

A good measure of the strength of inclusive  $\Lambda_c^\pm$  production for various scattering processes and kinematical conditions is the  $\Lambda_c^\pm/D^0$  production ratio. A detailed knowledge of this ratio, including its dependence on kinematic variables like  $p_T$  and  $y$ , should be sensitive to the fragmentation mechanism in the charm sector. Related important quantities characterizing the strength of the hadronization of a heavy quark into a hadron are the so-called fragmentation fractions defined by

$$B_Q(\mu) = \int_{x_{cut}}^1 dx D_Q(x, \mu), \quad (3)$$

and the average energy fractions

$$x_Q(\mu) = \frac{1}{B_Q(\mu)} \int_{x_{cut}}^1 dx x D_Q(x, \mu). \quad (4)$$

For the FFs constructed in Ref. [7], these fragmentation fractions in the next-to-leading order (NLO) fit turned out to be  $B_c(2m_c) = 0.0612$  and  $B_b(2m_b) = 0.143$ . The corresponding average momentum fractions for  $c, b \rightarrow \Lambda_c^+$  were found to be  $x_c(2m_c) = 0.738$  and  $x_b(2m_b) = 0.290$ . These are the values at threshold. Corresponding values at  $\mu = M_Z$  can be found in Ref. [7].

In principle, these quantities can be determined from integrated cross sections. However, data are usually available in a restricted phase space region only and an extrapolation to the full phase space is needed. In addition, experimental determinations are averaged over phase space in such a way that the (weak) scale dependence of  $B_Q$  and  $x_Q$  is lost.

Recently, a summary of experimental data for the fragmentation fractions of charm quarks into specific charmed hadrons was given in Ref. [13]. Measurements performed in photoproduction, deep inelastic  $e^\pm p$  scattering,  $pp$  collisions and  $e^+e^-$  annihilation were compared on the basis of up-to-date branching ratios for the respective decays of the final charmed hadrons. In that work, the average branching fraction for the transition  $c \rightarrow \Lambda_c^+$  in  $Z$  decays was found to be  $B_c = 0.060 \pm 0.0177$ . The value from Ref. [13] is based not only on OPAL measurements [8], but data from ALEPH and DELPHI were included as well. The branching fraction determined from other processes came out quite similar:  $B_c = 0.0540 \pm 0.0195$  (from  $e^\pm p$  DIS data),  $B_c = 0.067 \pm 0.0106$  (from photoproduction in  $e^\pm p$  scattering) and  $B_c = 0.0639 \pm 0.0122$  (from  $pp$  collisions at the LHC). Also  $\Lambda_c^\pm$  production in  $e^+e^-$  annihilation at a center-of-mass energy  $\sqrt{S} = 10.5$  GeV was analysed. The results are based on measurements performed by CLEO [14, 15], ARGUS [16], BABAR [17] and Belle [3]. From these data, the branching fraction  $B_c = 0.0611 \pm 0.0060$  was obtained. This value agrees with the one obtained directly by BABAR [17], i.e.  $B_c = 0.071 \pm 0.003 \pm 0.018$ , where the second error is due to the uncertainty of the branching fraction for the reconstructed decay mode. From the analysis of Ref. [13], we can conclude that all branching fractions agree very well between the different production channels. This is in contrast with corresponding observations in the  $b$ -quark sector, i.e. for fragmentation fractions of  $b \rightarrow \Lambda_b^0$  transitions [18]. There, data from the LEP and Tevatron experiments disagree and indicate a strong dependence on kinematic properties of the production process.

All these determinations are in good agreement with the value  $B_c(2m_c) = 0.0612$  obtained in the fit reported in Ref. [7]. However, we have to note that the value in Ref. [7] is connected with an obsolete value for the branching ratio  $\text{Br}(\Lambda_c^+ \rightarrow \pi^+ K^- p) = 0.044$  as it was known in 1996, while the recent PDG value is  $\text{Br}(\Lambda_c^+ \rightarrow \pi^+ K^- p) = 0.0635$  [1]. The agreement is therefore fortuitous.

In the following, we present predictions for the production of  $\Lambda_c^\pm$  in the LHC experiments, first using the FF fit based only on the high-energy LEP data from OPAL [8]. Then, a new fit where we include also  $e^+e^- \rightarrow \Lambda_c^\pm + X$  data at  $\sqrt{S} = 10.5$  GeV from Belle [19] and corresponding predictions for the LHC will be presented.

The outline of the paper is as follows. In Sect. 2, we introduce our strategy for the calculation of cross sections for inclusive  $\Lambda_c^\pm$  production in the LHCb, ALICE and CMS experiments. In Sect. 3, we present numerical results for the  $p_T$ -differential cross sections and compare them with these three LHC experiments. These calculations are performed using the old FF of Ref. [7] to describe the transition of  $c$  and  $b$  quarks to  $\Lambda_c^+$ . A new FF set obtained from a fit to the OPAL data [8] and the new measurements from Belle at  $\sqrt{S} = 10.52$  GeV [19] are then described in Sect. 4. This new FF is used in Sect. 5 for a calculation of  $d\sigma/dp_T$  for  $\Lambda_c^\pm$  production and compared with the LHC data. A discussion

of our findings and conclusions are presented in Sect. 5.

## 2 Setup and input

The theoretical description of the GM-VFNS framework as well as technical details of its implementation can be found in Refs. [20, 21]. Here we describe only the input required for the numerical computations for which the results are given in the next section. For the proton PDF, we use CTEQ14 [22] as implemented in the LHAPDF library [23]. We take the  $c$ -quark pole mass to be  $m_c = 1.3$  GeV, in agreement with the value assumed for the PDF set CTEQ14. The strong coupling  $\alpha_s^{(n_f)}(\mu_R)$  is evaluated at NLO with  $\Lambda_{\overline{\text{MS}}}^{(4)} = 328$  MeV. This corresponds to  $\Lambda_{\overline{\text{MS}}}^{(5)} = 225$  MeV above the 5-flavour threshold chosen at  $m_b = 5$  GeV.

In the following sections, we shall take equal values for the initial- and final-state factorization scales  $\mu_F$ , entering the PDFs and FFs, respectively. We choose  $\mu_F$  and the renormalization scale  $\mu_R$  at which  $\alpha_s$  is evaluated as

$$\mu_F = 0.98\mu_T, \quad \mu_R = \xi_R\mu_T, \quad (5)$$

with  $\mu_T = 0.5\sqrt{p_T^2 + 4m_c^2}$  and  $m_c = 1.3$  GeV. Theoretical uncertainties will be estimated by varying  $\xi_R$  in the range between 1/2 and 2. This choice, in particular for  $\mu_F$ , allows us to obtain realistic predictions for  $p_T$  values also below 3 GeV, as needed to compare with the complete data set of the LHCb collaboration as well as with ALICE data. The choice in Eq. (5) for  $\mu_F$  was first applied in Ref. [24], where we found it instrumental to obtain good agreement with inclusive  $D$ -meson cross sections  $d\sigma/dp_T$  for  $p_T$  values down to  $p_T = 0$ .

First, we shall use the non-perturbative  $\Lambda_c^+$  FFs constructed in our earlier work [7]. These FFs have been fitted only to inclusive ( $\Lambda_c^+ + c.c.$ ) production data in  $e^+e^-$  annihilation on the  $Z$  resonance measured by the OPAL collaboration at LEP1 [8]. The starting scale was fixed at  $\mu_0 = 1.5$  GeV. In a subsequent section, we shall describe a new  $\Lambda_c^+$  FF obtained from a fit to data which include, in addition to the old OPAL data,  $e^+e^-$  data at  $\sqrt{S} = 10.52$  GeV from the Belle collaboration [19].

## 3 Comparison with LHCb, ALICE and CMS data using old FFs

The first measurements of the cross section for inclusive  $\Lambda_c^\pm$  production in  $pp$  collisions at the LHC were performed some time ago by the LHCb collaboration [10]. These measurements provided data for differential cross sections  $d\sigma/dp_T$  for  $\Lambda_c^+ + c.c.$  baryons in bins of  $p_T$ , integrated over the forward rapidity range  $2.0 < y < 4.5$ . In addition, cross sections in bins of  $y$  integrated over the  $p_T$  range  $2 < p_T < 8$  GeV were presented. The  $p_T$ -bin

integrated cross sections were compared with our GM-VFNS calculations using the  $\Lambda_c^+$  FFs of Ref. [7] for  $p_T \geq 3$  GeV. These GM-VFNS predictions agreed fairly well with the LHCb data [10].

Our previous calculation of the  $\Lambda_c^\pm$  production cross section was performed with a choice of the renormalization and factorization scales which forced us to restrict ourselves to large  $p_T$ . To improve this, we repeat these calculations with the same  $\Lambda_c^+$  FF of Ref. [7], but now using the scale parameters as described in Sect. 2. The cross sections  $d\sigma/dp_T$  compared with the LHCb data [10] are shown in Fig. 1, left side. We have rescaled these data<sup>1</sup> to be consistent with a more recent value for the branching ratio of the  $\Lambda_c^+ \rightarrow \pi^+ K^- p$  decay [1] (factor 0.7874). The data thus obtained lie inside the theory uncertainty band which is obtained from scale variations for  $\mu_R$  using scale factors  $\xi_R$  ranging from 0.5 to 2.0. The ratio of data over theory is presented in Fig. 1, right side. For the default scale  $\xi_R = 1.0$ , it agrees with unity inside the experimental errors. The error bars for the data are only shown for the central curve (full line) corresponding to  $\xi_R = 1.0$ . The histograms with dashed lines correspond to  $\xi_R = 0.5$  and  $\xi_R = 2.0$ .

In order to obtain ratios of  $\Lambda_c^+$  over  $D^0$  production, we calculate the cross section for inclusive  $D^0$  production with the same kinematical conditions and with the same choice of

---

<sup>1</sup> This rescaling is needed only for the LHCb data. The data analyses of ALICE and CMS to be discussed below have already used the more recent value of the branching ratio for the  $\Lambda_c^\pm$  decays.

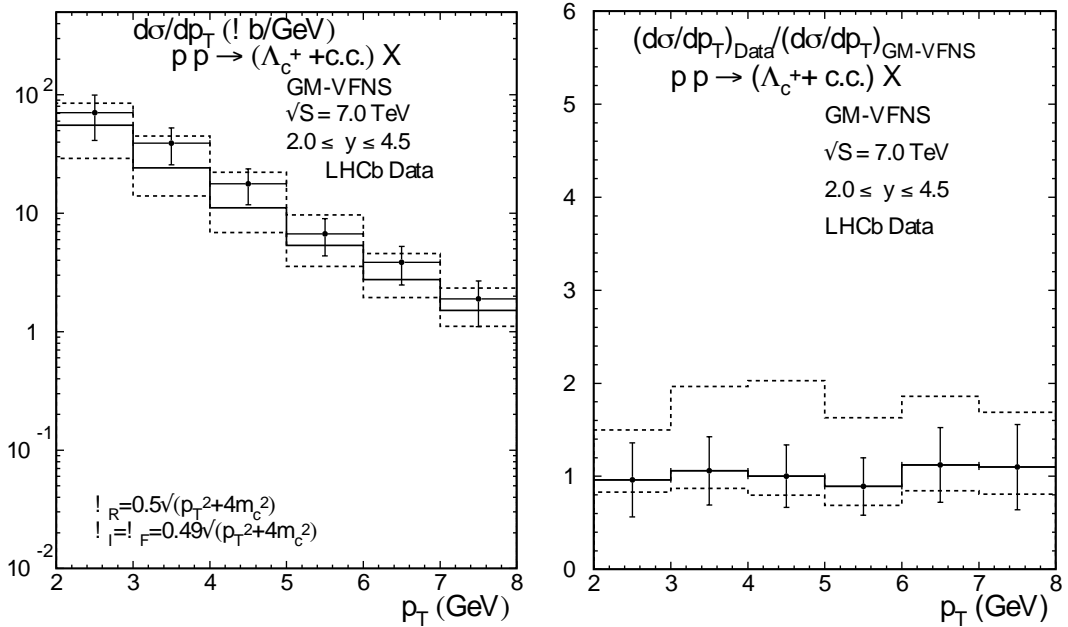


Figure 1: Differential  $\Lambda_c^\pm$  production cross sections at  $\sqrt{S} = 7$  TeV as a function of  $p_T$  compared with LHCb data. The right plot shows the ratio of data over theory. The dashed histograms indicate the scale uncertainty for  $0.5 \leq \xi_R \leq 2.0$ .

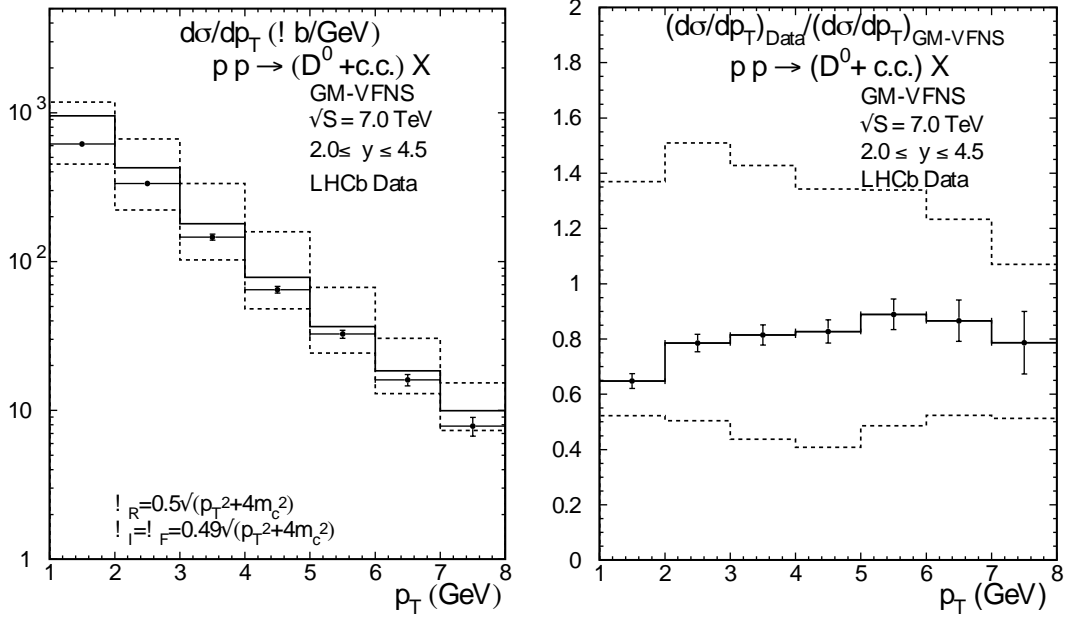


Figure 2: Differential  $D^0$  production cross sections at  $\sqrt{S} = 7$  TeV as a function of  $p_T$  compared with LHCb data. The right plot shows the ratio of data over theory. The dashed histograms indicate the scale uncertainty for  $0.5 \leq \xi_R \leq 2.0$ .

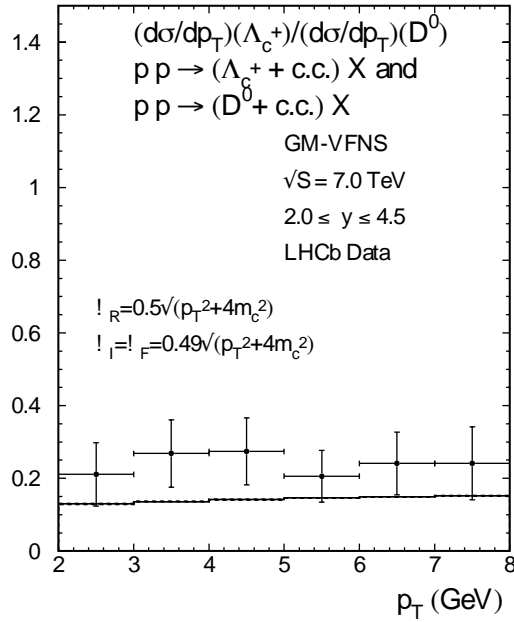


Figure 3:  $\Lambda_c^\pm$  to  $D^0$  ratio of production cross sections at  $\sqrt{S} = 7$  TeV as a function of  $p_T$  compared with LHCb data.

scales  $\mu_F$  and  $\mu_R$  as for  $\Lambda_c^\pm$ . They include the inclusive production of both charge-conjugate states,  $D^0 + c.c.$ , as given in the LHCb publication [10]. The predictions are compared with the data [10] for  $\sqrt{S} = 7$  TeV. We find agreement within the theory uncertainty band given by the scale variation (see Fig. 2, left side). The ratio of data over theory, shown in the right panel of Fig. 2, is approximately 0.8. Experimental uncertainties are rather small, and the deviation of this ratio from unity is quite significant, but agrees with theory within the larger theory uncertainties. Using these results, we can now calculate the ratio of  $\Lambda_c^\pm$  and  $D^0$  cross sections as a function of  $p_T$ . The result is shown in Fig. 3. The predicted ratio is approximately equal to 0.15 and below the experimental value of  $\simeq 0.2$  by about one standard deviation of the experimental errors. One should note that the scale dependence of the theory prediction cancels to a good degree in the ratio of cross sections. The dependence on PDF uncertainties is expected to be much smaller than the scale dependence [25] and would also cancel to some extent in the ratio of cross sections.

We repeat these calculations to compare with ALICE data [11]. These data have been obtained for central production  $|y| \leq 0.5$  at  $\sqrt{S} = 7$  TeV and in five  $p_T$  bins between 1 GeV and 8 GeV. One should note that these data are for inclusive  $\Lambda_c^\pm$  production without including charge-conjugate states, in contrast to data from the LHCb collaboration. We choose the prescription of Eq. (5) to fix the renormalization and factorization scales. The results are shown in Fig. 4, left side, and compared with the ALICE measurements [11]. For all five  $p_T$  bins the data are larger than our predictions and outside the theory error

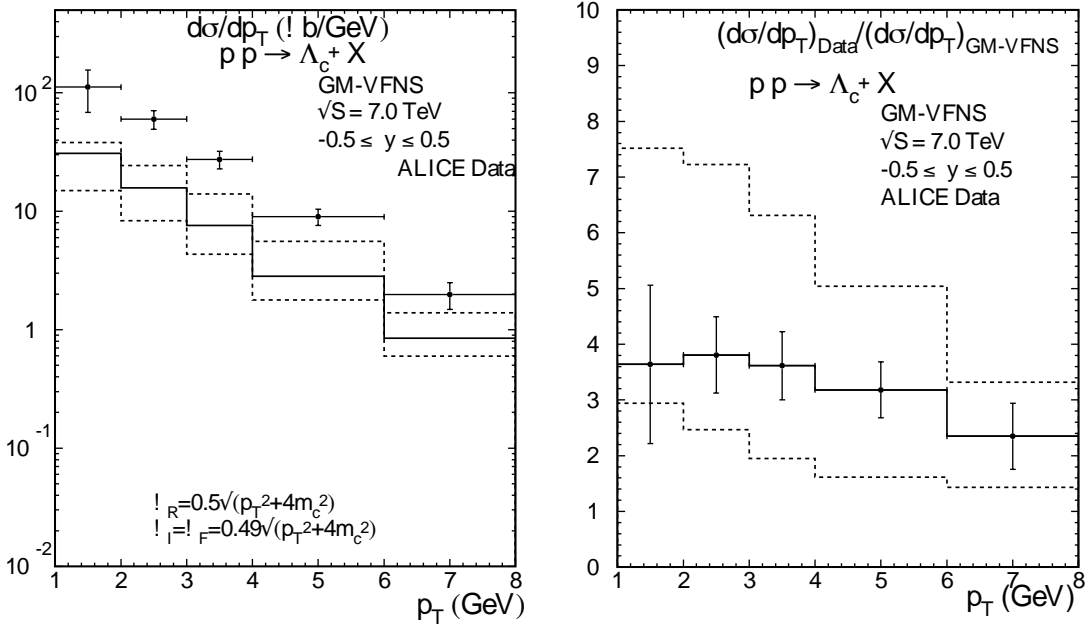


Figure 4: Differential  $\Lambda_c^\pm$  production cross sections at  $\sqrt{S} = 7$  TeV as a function of  $p_T$  compared with ALICE data. The right plot shows the ratio of data over theory. The dashed histograms indicate the scale uncertainty for  $0.5 \leq \xi_R \leq 2.0$ .



band due to scale variations. The ratio of data over GM-VFNS results, shown in Fig. 4, right side, ranges between  $3.6 \pm 1.4$  (in the bin with smallest  $p_T$ ) and  $2.4 \pm 0.6$  (in the bin with largest  $p_T$ ). This agrees with the comparison shown in Ref. [11], where predictions with a different choice of scales have been used. These results show, as already stated in the ALICE publication [11], that the measured cross sections in the central  $|y|$  region are much larger than the predictions. In contrast, as shown above, the LHCb results in the forward  $y$  region are compatible with predictions based on the  $\Lambda_c^+$  FF from Ref. [7].

To obtain the  $\Lambda_c^+/D^0$  ratio, we need the inclusive  $D^0$  cross sections, again for the same bin sizes and with the same choice of scales. Results are shown in Fig. 5, left side, and compared with ALICE data taken from Refs. [26, 27]. The experimental data fall inside the uncertainty band due to  $\xi_R$  variation in the range  $1/2 < \xi_R < 2$ , where the lower value of  $\xi_R$  leads to the maximum prediction. The full-line histogram is for the default choice  $\xi_R = 1.0$ . It agrees fairly well with the experimental data. The ratio of data over theory is shown in Fig. 5, right side. This ratio is approximately equal to unity. The comparison of data and theory for the  $\Lambda_c^+/D^0$  cross section ratio is shown in Fig. 6. One can see clearly a disagreement between data and prediction. Experimental values for this ratio are found to range between 0.6 (at small  $p_T$ ) and 0.4 (at large  $p_T$ ). They exceed the theoretical prediction by factors of approximately 4.0 at small  $p_T$  and 2.7 at large  $p_T$ . Theory predicts a value of  $\simeq 0.15$ , which is independent of the scale choice. Comparing Figs. 4 and 5, it is obvious that the discrepancy seen in the  $\Lambda_c^+/D^0$  ratio originates solely from the  $\Lambda_c^\pm$  cross

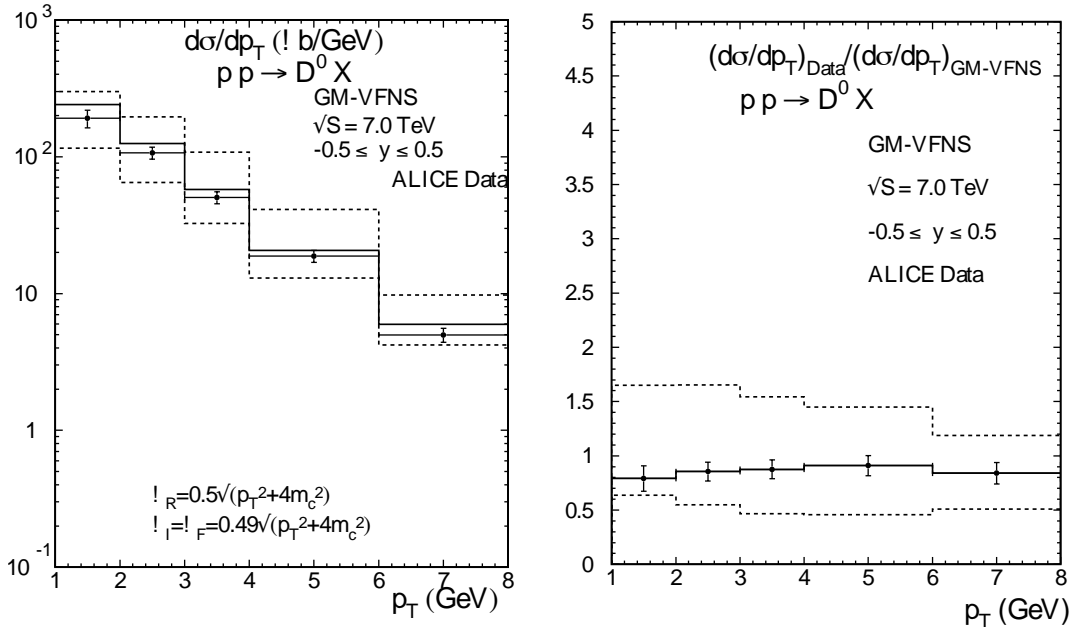


Figure 5: Differential  $D^0$  production cross sections at  $\sqrt{S} = 7$  TeV as a function of  $p_T$  compared with ALICE data. The right plot shows the ratio of data over theory. The dashed histograms indicate the scale uncertainty for  $0.5 \leq \xi_R \leq 2.0$ .

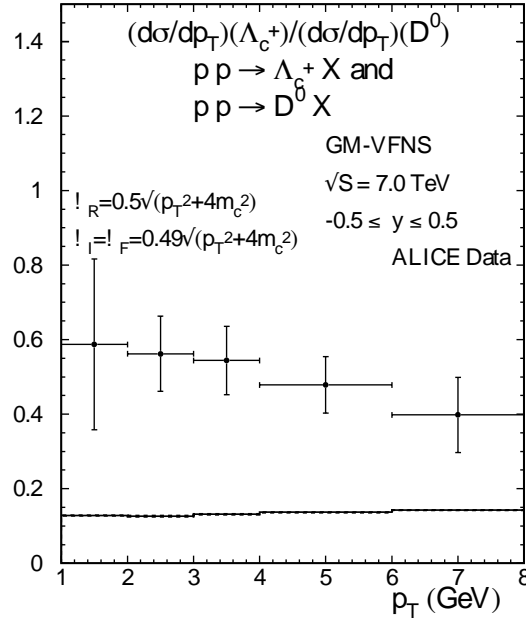


Figure 6:  $\Lambda_c^+$  to  $D^0$  ratios of production cross sections at  $\sqrt{S} = 7$  TeV as a function of  $p_T$  compared with ALICE data.

section.

Finally, we present results for  $\Lambda_c^\pm$  and  $D^0$  production at  $\sqrt{S} = 5.02$  TeV, which we compare with the recent CMS measurements [12]. Data from CMS are available for  $d\sigma/dp_T$  in four  $p_T$  bins in the range between 5 and 20 GeV, and in the rapidity interval  $|y| < 1.0$ . This kinematic range is similar to the one of the ALICE measurements [11]. Both cover the central rapidity range, somewhat larger in the case of CMS ( $|y| < 1.0$ ) than in the case of ALICE ( $|y| < 0.5$ ). Our results are shown in Fig. 7, left side, and compared with the four data points from CMS [12]. The ratio of data over GM-VFNS predictions is presented in Fig. 7, right side, and agrees with unity at the lower border of the uncertainty band due to scale variations, i.e. within theory errors. The results of  $d\sigma/dp_T$  for  $D^0$  production in the same  $p_T$  bins are shown in Fig. 8, left side. Our results are compared with CMS data, which we have taken from the corresponding figure in Ref. [28]. We find a very good agreement between data and the calculation using default scales. The ratio of data over theory shown in Fig. 8, right side is equal to unity, as expected. The ratio of  $d\sigma/dp_T$  for  $\Lambda_c^+$  over  $D^0$  production is shown in Fig. 9. Theory predicts a ratio of  $\simeq 0.15$ , a result similar to the one obtained for the LHCb kinematic range shown in Fig. 5, i.e. theory does not predict for this ratio a strong dependence on the rapidity range. The CMS data for the  $\Lambda_c^+/D^0$  ratio shown in Fig. 9 is approximately 0.3, only a factor two larger than the theoretical result. The data point for the bin  $6 < p_T < 8$  GeV in Fig. 9 can be compared with a data point in the same  $p_T$  bin from ALICE, see Fig. 6. The two data differ only by the different sizes of the  $y$  coverage. The ALICE point is found at a value of  $0.4 \pm 0.1$ ,

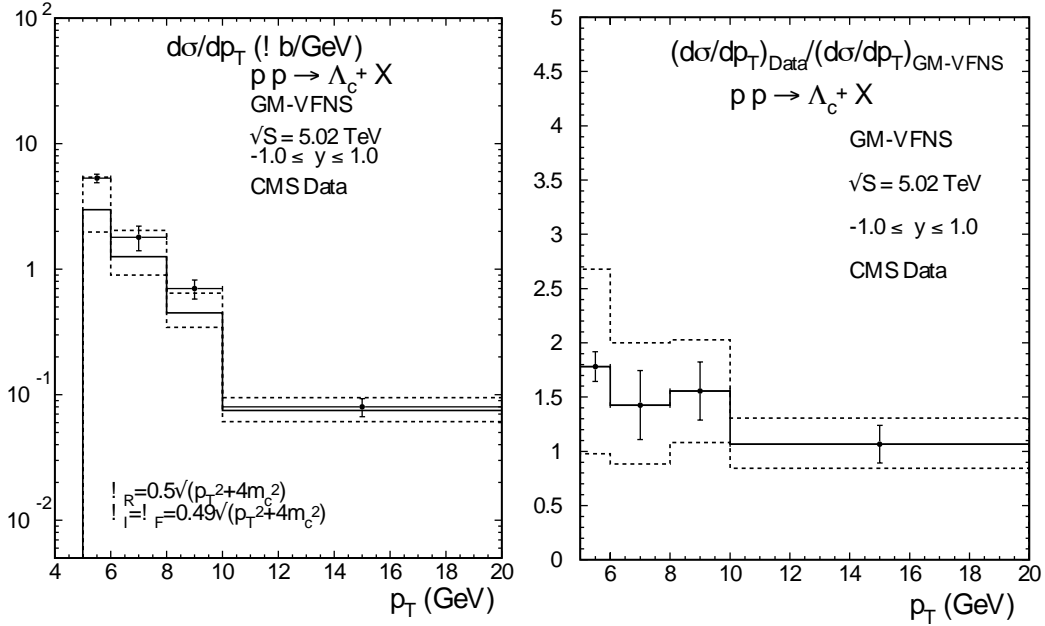


Figure 7: Differential  $\Lambda_c^\pm$  production cross sections at  $\sqrt{S} = 5.02$  TeV as a function of  $p_T$  compared with CMS data. The right plot shows the ratio of data over theory. The dashed histograms indicate the scale uncertainty for  $0.5 \leq \xi_R \leq 2.0$ .

whereas the data point in Fig. 9 from CMS is at  $0.265 \pm 0.112$ , somewhat below the ALICE value. It is unclear whether this difference can be attributed to the smaller  $|y|$  range for the ALICE point.

Comparing the theory predictions for the ratio of cross sections for  $\Lambda_c^\pm$  and  $D^0$  production shown in Figs. 3, 6 and 9, we can see that they are very similar; there is neither an indication for a strong dependence on rapidity, nor on the range of  $p_T$  values which have been investigated by the three experiments, LHCb ( $2 < p_T < 8$  GeV), ALICE ( $1 < p_T < 8$  GeV) and CMS ( $5 < p_T < 20$  GeV). We should expect that also the measured  $\Lambda_c^+/D^0$  ratios in the three experiments should be equal. This is, however, not the case. The data for the  $\Lambda_c^+/D^0$  ratio measured by LHCb and CMS are almost equal inside their large experimental uncertainties,  $\simeq 0.3$  for both experiments. In contrast, the values found by ALICE are larger. This discrepancy is most significant at small  $p_T$ , where the ALICE value of the ratio is  $\sim 0.6$ , while their value  $\sim 0.4$  at large  $p_T$  comes closer to the results from the LHCb and CMS collaborations.

The situation is different in the case of  $b$ -hadron production. In a previous work [18] we have compared predictions for  $\Lambda_b^0$  production with data from the LHCb collaboration. At small  $p_T$ , the ratio of  $\Lambda_b^0$  to  $B^0$  production cross sections was in agreement with theory, which is essentially determined by the ratio of the  $b \rightarrow \Lambda_b^0$  to  $b \rightarrow B$  fragmentation fractions,  $f_{\Lambda_b}/f_d \simeq 0.25$ . Only at  $p_T \gtrsim 10$  GeV, the LHCb data of this ratio decrease and reach the value 0.15 at  $p_T \simeq 20$  GeV, which is about 2 to  $3\sigma$  below the expected value.

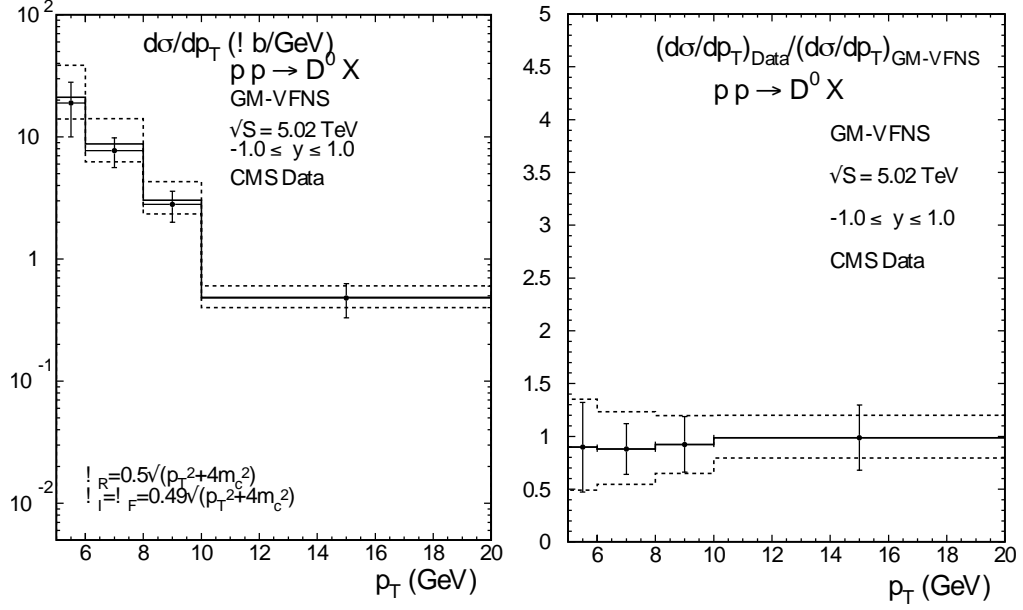


Figure 8: Differential  $D^0$  production cross sections at  $\sqrt{S} = 5.02$  TeV as a function of  $p_T$  compared with CMS data. The right plot shows the ratio of data over theory. The dashed histograms indicate the scale uncertainty for  $0.5 \leq \xi_R \leq 2.0$ .

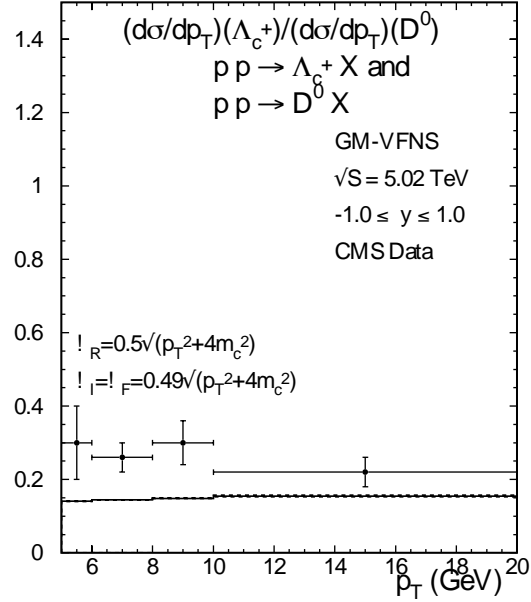


Figure 9:  $\Lambda_c^+$  to  $D^0$  ratio of production cross sections at  $\sqrt{S} = 5.02$  TeV as a function of  $p_T$  compared with CMS data.

## 4 New fit of the $\Lambda_c^+$ FF

The old FF parametrization used in the previous section was based on a fit to OPAL data [8] including only 4 points with rather large uncertainties. Here we describe a new fit including Belle data at  $\sqrt{S} = 10.52$  GeV [19]. The Belle data set is much more precise and contains more points. Only 35 of the available total number of 42 points will be used in our fit, since we have to exclude data at small values of the scaling variable  $x$ , where theory is not reliable without taking resummation of soft-gluon logarithms into account.

The combination of old OPAL data with the more recent data from Belle requires special care, since the two experiments have based their analyses on the observation of the decay  $\Lambda_c^+ \rightarrow \pi^+ K^- p$  for which different branching ratios have been used. OPAL has used the 1996 value  $\text{Br}(\Lambda_c^+ \rightarrow \pi^+ K^- p) = 0.044$  [8], whereas the analysis of the Belle measurements relies on the world average  $\text{Br}(\Lambda_c^+ \rightarrow \pi^+ K^- p) = 0.0635$  from the 2016 Review of Particle Physics [29]. We, therefore, re-scale the OPAL cross sections by the factor  $0.044/0.0635 = 0.6929$ . The branching fractions for the transitions  $c \rightarrow \Lambda_c^+$  and  $b \rightarrow \Lambda_c^+$  are correspondingly reduced by this factor.

The strategy for constructing the  $\Lambda_c^+$  FF is the same as in our previous work with T. Kneesch for  $D$ -meson FFs [4]. The  $e^+e^-$  annihilation cross sections are calculated at NLO with corrections for non-zero charm and bottom masses. Corrections for the finite mass of the charmed baryon  $\Lambda_c^\pm$  are also taken into account. We parametrize the  $x$ -dependence of the  $c$ - and  $b$ -quark FFs at their respective starting scales as suggested by Bowler [30]:

$$D_Q(x, \mu_0) = N x^{-(1+\gamma)^2} (1-x)^a e^{-\gamma^2/x}, \quad (6)$$

with three parameters  $N$ ,  $a$  and  $\gamma$  for each of the quarks  $Q = c, b$ . The starting scales are  $\mu_0 = 1.5$  GeV for  $Q = c$  and  $\mu_0 = 5$  GeV for  $Q = b$ . The fitting procedure is as follows. At the starting scale  $\mu_0 = 1.5$  GeV the  $c$ -quark FF is taken to be of the form given in Eq. (6), while the FFs of the light quarks  $u, d, s$  and the gluon are set equal to zero. Then these FFs are evolved to higher scales using the DGLAP evolution equations (see, for example, Eq. (10) in Ref. [4]) at NLO with  $n_f = 4$  active quark flavors and a given value of  $\Lambda_{\overline{\text{MS}}}^{(4)}$ . When the scale reaches the bottom threshold at  $\mu_F = m_b = 5$  GeV, the bottom flavour is activated and its FF is introduced in the Bowler form of Eq. (6). The evolution to higher scales is performed with  $n_f = 5$  and the value  $\Lambda_{\overline{\text{MS}}}^{(5)}$  is properly adjusted to match the value of  $\Lambda_{\overline{\text{MS}}}^{(4)}$ . We also note that, in Ref. [19], the Belle collaboration has provided data which are corrected for radiative effects. We use these data and thus do not have to apply radiative corrections ourselves, as described in Ref. [4].

Similarly to the work in Ref. [4], we perform three different fits. First, FFs are determined using separately the  $B$ -factory data (Belle fit) and the rescaled  $Z$ -factory data (OPAL fit). Then we obtain a common fit (global fit) combining the two data sets.

We start by updating the FF fit to the OPAL data using the rescaled cross sections to match the up-to-date value of  $\text{Br}(\Lambda_c^+ \rightarrow \pi^+ K^- p)$ . There are two data sets coming from

	OPAL	Belle	global
$N_c$	80345	$1 \times 10^{10}$	$1 \times 10^{10}$
$a_c$	$0.35431 \times 10^{-6}$	2.1828	2.1821
$\gamma_c$	3.6432	4.5391	4.5393
$N_b$	19.953	19.953	41.973
$a_b$	6.3031	6.3031	7.4092
$\gamma_b$	1.1773	1.1773	1.2457
$\chi^2/\text{d.o.f}$	0.4749	3.2928	2.8030

Table 1: Values of fit parameters resulting from the OPAL, Belle and global fits in the GM-VFNS approach together with the value of  $\chi^2$  per degree of freedom.

FF set	$B_c(10.52 \text{ GeV})$	$B_c(M_Z)$	$B_b(10.52 \text{ GeV})$	$B_b(M_Z)$
OPAL	—	$4.1739 \times 10^{-2}$	—	$8.2474 \times 10^{-2}$
Belle	$6.6476 \times 10^{-2}$	—	$8.9244 \times 10^{-2}$	—
global	$6.6435 \times 10^{-2}$	$6.4452 \times 10^{-2}$	$8.3220 \times 10^{-2}$	$7.7197 \times 10^{-2}$

Table 2: Values of  $c \rightarrow \Lambda_c^+$  and  $b \rightarrow \Lambda_c^+$  fragmentation fractions at  $\mu_f = 10.52 \text{ GeV}$  and  $\mu_f = M_Z$ .

OPAL [8]: one sample includes only  $\Lambda_c^\pm$  baryons produced in the decays of  $b$  hadrons from  $Z \rightarrow b\bar{b}$  (denoted  $b$ -tagged); a second sample includes in addition  $\Lambda_c^\pm$  baryons from the direct production in  $Z \rightarrow c\bar{c}$  events and from light-quark and gluon fragmentation (denoted total). We determine the FFs for  $c \rightarrow \Lambda_c^+$  and  $b \rightarrow \Lambda_c^+$  in a common fit. The resulting values of the fit parameters and the  $\chi^2$  per degree of freedom are given in Table 1 in the column denoted “OPAL”. The quality of the fit may be judged from Fig. 10 (left). The fragmentation fractions for  $c \rightarrow \Lambda_c^+$  and  $b \rightarrow \Lambda_c^+$  resulting from this fit at  $\mu_F = 10.52 \text{ GeV}$  are listed in Table 2 and the average energy fractions in Table 3. Compared with our previous fit [7], these values have changed as expected.

In the Belle data [19], contributions from  $B$ -meson decays are excluded, so that the  $b \rightarrow \Lambda_c^+$  FF is not needed in the calculation of cross sections. However, the FFs from  $c$  and  $b$  quarks are coupled through the DGLAP evolution. We fix the  $b \rightarrow \Lambda_c^+$  FF using the values of  $N_b$ ,  $a_b$  and  $\gamma_b$  obtained from the OPAL fit. The fit to the Belle data yields new values for  $N_c$ ,  $a_c$  and  $\gamma_c$ , which are shown in the column denoted “Belle” in Table 1. The corresponding values for the fragmentation and average energy fractions are given in Tables 2 and 3, respectively.

Finally, in our global fit, we use all available data for inclusive  $\Lambda_c^+ + c.c.$  production in  $e^+e^-$  annihilation from Belle and OPAL. The resulting values of the fit parameters and of  $\chi^2$  are included in Table 1, and the resulting fragmentation and average energy fractions are found in Tables 2 and 3, respectively. The result of the global fit is compared with OPAL

FF set	$x_c(10.52 \text{ GeV})$	$x_c(M_Z)$	$x_b(10.52 \text{ GeV})$	$x_b(M_Z)$
OPAL	—	0.5389	—	0.2717
Belle	0.5685	—	0.3063	—
global	0.5685	0.4868	0.3009	0.2666

Table 3: Values of average energy fractions for  $c \rightarrow \Lambda_c^+$  and  $b \rightarrow \Lambda_c^+$  transitions at  $\mu_f = 10.52 \text{ GeV}$  and  $\mu_F = M_Z$ .

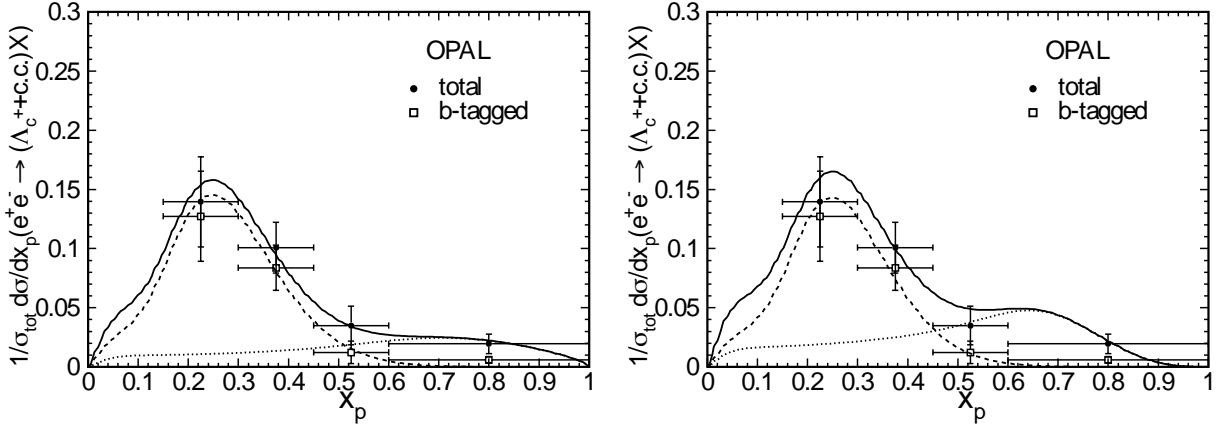


Figure 10: OPAL fit (left) and global fit (right) compared with OPAL data. The dashed line shows the contribution originating from  $b$ -quark production, the dotted line describes the  $c$  component and the full line is the sum of both contributions to the normalized production cross section.

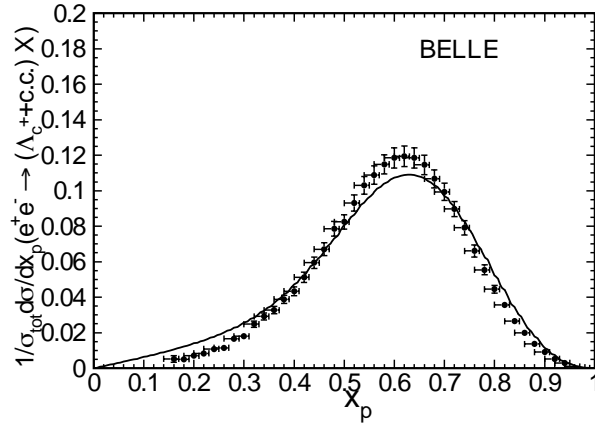


Figure 11: Result of the global fit for the normalized  $\Lambda_c^+ + c.c.$  production cross section compared with Belle data.

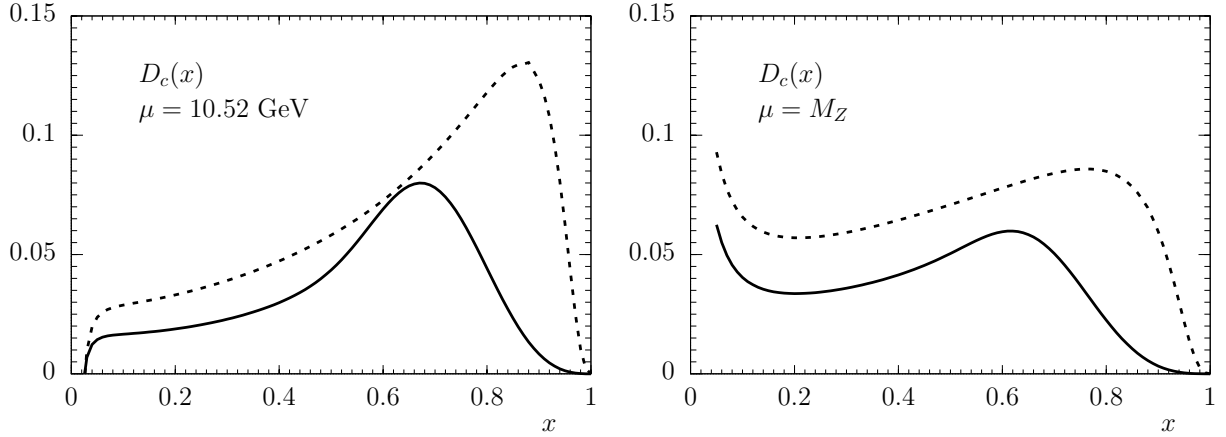


Figure 12: The fragmentation function for  $c \rightarrow \Lambda_c^+$  at scales  $\mu = 10.52$  GeV (left) and  $\mu = M_Z$  (right). The full curves show the new fit described in this work, the dashed lines represent the fit of Ref. [7].

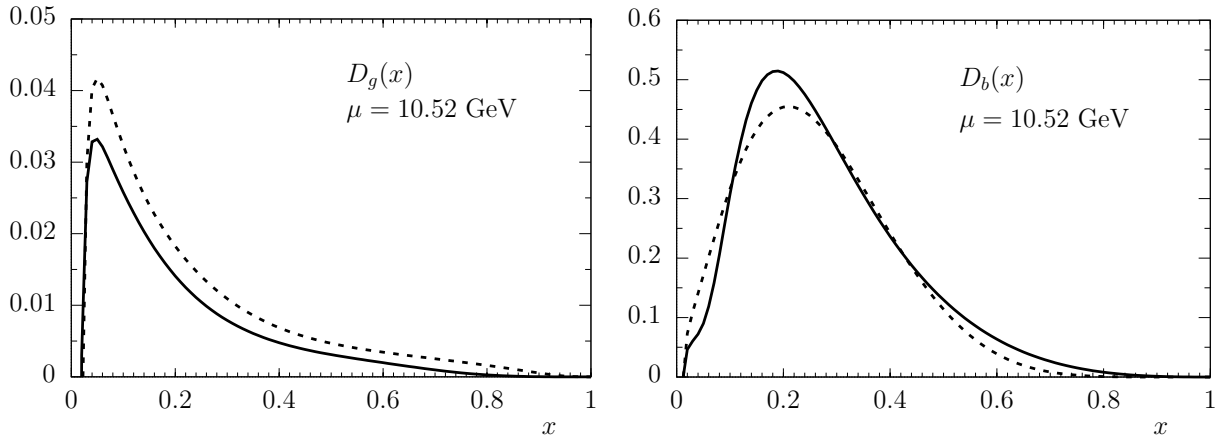


Figure 13: The fragmentation function for  $g \rightarrow \Lambda_c^+$  (left) and  $b \rightarrow \Lambda_c^+$  (right) at  $\mu = 10.52$  GeV. The full curves show the new fit described in this work, the dashed lines represent the fit of Ref. [7].

data in Fig. 10 (right). Compared with the OPAL fit, i.e. without the Belle data, shown in the left part of Fig. 10, the global fit has a larger  $c \rightarrow \Lambda_c^+$  component. The comparison of the global fit with the Belle data is shown in Fig. 11. The quality of the fit is obviously not perfect. This might be connected to the fact that the Bowler ansatz for the heavy-quark FFs contains only three free parameters and, therefore, is not flexible enough. It is clear that the Belle data dominate the fit, since this data set contains many more data points with smaller uncertainties. This is also reflected by the values of the  $c \rightarrow \Lambda_c^+$  fragmentation fraction shown in Table 2. We, therefore, do not show a separate figure with a comparison of the Belle fit with Belle data, since it would be almost indistinguishable from Fig. 11.



A direct comparison of the old and new FFs is shown in Figs. 12 and 13. We note that both shape and normalization of  $D_c(x)$  have changed. The maxima of the new FFs appear at smaller values of  $x$ . The normalization is reduced, since we have rescaled the OPAL data by the factor 0.6929 to match the new branching ratio of the  $\Lambda_c^+ \rightarrow \pi^+ K^- p$  decay. The differences between the two fits for the  $D_g$  and  $D_b$  FFs (Fig. 13) are smaller. We note that the  $g \rightarrow \Lambda_c^+$  FF has its maximum at rather low  $x$  and does therefore not play an important role for the comparison with the available  $e^+e^-$  data which, in turn, means that  $D_g(x)$  is not well constrained by these data. One would need to perform fits to  $pp$  data in order to improve our knowledge of the gluon FF.

## 5 $\Lambda_c^\pm$ production with new FF and comparison with LHC data

The FFs obtained in the fits described in the previous section have been converted into a grid, which subsequently is used for the calculation of inclusive  $\Lambda_c^\pm$  production cross sections in  $pp$  collisions at the LHC to be compared with data from LHCb, ALICE and CMS measurements. Corresponding results are presented now.

In Fig. 14, our results are compared with data from the LHCb, ALICE and CMS collaborations in the same way as this was done in Figs. 1, 4 and 7 (left sides). The predicted cross sections for the three experiments come out similar to the earlier results in the previous section, but are slightly smaller. For example, the LHCb cross section in Fig. 14 is smaller than the one in Fig. 1 by approximately 15 % in the first  $p_T$  bin and 35 % in the last  $p_T$  bin. The reduction of the cross section  $d\sigma/dp_T$  is similar for ALICE and CMS (see upper right and lower panels of Fig. 14). This means that also the  $\Lambda_c^+/D^0$  ratio is reduced by about the same amount when using the new FFs. This change is not very large, and the comparison of theory predictions with data is qualitatively the same with the new FF. For the LHCb data (Fig. 14, upper left panel) and for the CMS data (Fig. 14, lower panel) the measured cross sections  $d\sigma/dp_T$  for  $\Lambda_c^\pm$  production are still very close to the upper border of the theory uncertainty band. Only the ALICE data (Fig. 14, upper right panel) are significantly higher, by factors of 2 to 4, than the cross sections predicted from theory. It is very unlikely that this large discrepancy can be explained in the usual framework by realistic FFs for the  $\Lambda_c^\pm$  without destroying agreement with other data. This suggests that the ALICE data violate predictions based on the universality of the fragmentation process by a large factor, whereas the data from LHCb [10] and CMS [12] appear to be compatible with universality.

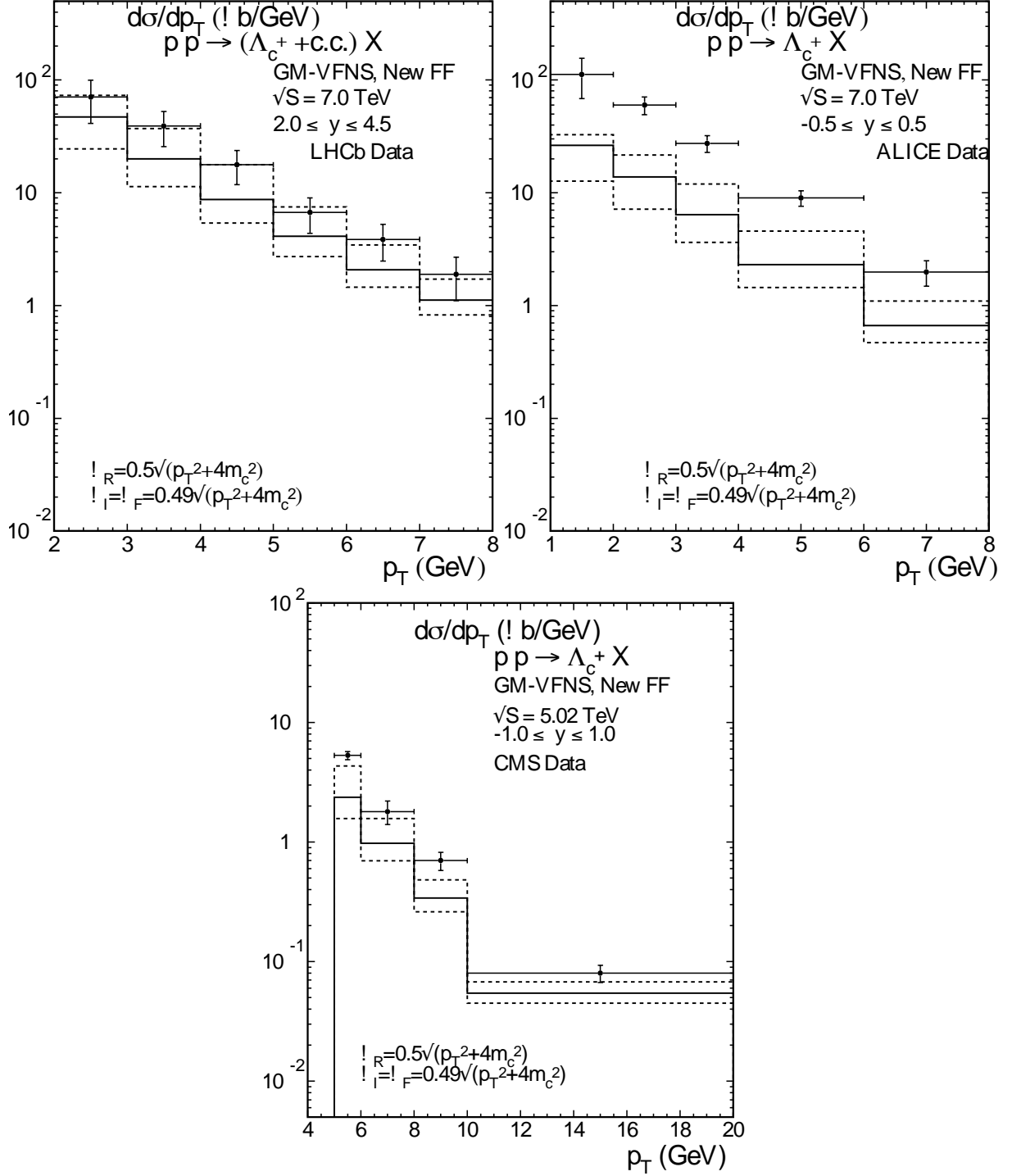


Figure 14: Differential  $\Lambda_c^\pm$  production cross sections evaluated with the new FF fit compared with data from LHCb (upper left), ALICE (upper right) and CMS (lower).

## 6 Discussion and summary

In Ref. [31], an attempt was made to explain the large  $\Lambda_c^+/D^0$  ratio seen in the ALICE measurements as arising from processes where  $\Lambda_c^+$  is produced from the decay of excited charm baryon states, which are not seen in the Belle data of  $e^+e^-$  annihilation. Actually, in the Belle data, only about 50% of the  $\Lambda_c^\pm$  production rate originates from direct  $c \rightarrow \Lambda_c^+$  fragmentation; the other half is due to decays of excited charm baryon states. However, it is difficult to understand that this fraction should be larger in  $pp$  collisions by a large factor, or that the production strength of the higher resonances discovered already in the Belle experiment should be so much larger in the ALICE  $pp$  collision experiment. This is an experimental question which could be answered only in the respective experiments.

Another possibility to enhance inclusive  $\Lambda_c^\pm$  production in  $pp$  collisions is suggested by models that include colour reconnection mechanisms [32] in the usual PYTHIA hadronization scheme. This implies that the final partons in the string fragmentation are considered to be colour-connected in such a way that the total string length becomes as short as possible. In Ref. [12], it is shown that this model is consistent with the CMS result for the  $\Lambda_c^+/D^0$  ratio, but it is not sufficient to explain the strong enhancement of this ratio in the ALICE data [11].

It seems unlikely that higher-order corrections, which go beyond the available NLO calculations, could help to obtain a better agreement of data with theory. NNLO fits for  $D$ -meson FFs have been studied recently in Refs. [33, 34]. However, such corrections are expected to affect all measurements in a similar way. Also alternative approaches like  $k_t$ -factorization [35], are not able to explain the observed discrepancies. The different coverage of kinematic variables,  $p_T$  and  $y$ , is not very different in the available data sets. On the experimental side, however, more data differential both in  $p_T$  and  $y$  would be extremely helpful, at least to clarify that data from different experiments are compatible with each other in the kinematic regions where they overlap.

## Acknowledgment

We thank M. Niiyama for providing us with data of the Belle experiment in numerical form. I.S. would like to acknowledge the Mainz Institute of Theoretical Physics (MITP) for its hospitality and support. The work of B.A.K. was supported in part by the German Federal Ministry for Education and Research BMBF through Grant No. 05H18GUCC1 and by the German Research Foundation DFG through Research Unit FOR 2926 “Next Generation Perturbative QCD for Hadron Structure: Preparing for the Electron-Ion Collider” with Grant No. KN 365/14-1.

## References

- [1] M. Tanabashi *et al.* [Particle Data Group], Phys. Rev. D **98** (2018) 030001.
- [2] Y. Amhis *et al.* [HFLAV Collaboration], Eur. Phys. J. C **77** (2017) 895 [arXiv:1612.07233 [hep-ex]].
- [3] R. Seuster *et al.* [Belle Collaboration], Phys. Rev. D **73** (2006) 032002 [hep-ex/0506068].
- [4] T. Kneesch, B. A. Kniehl, G. Kramer and I. Schienbein, Nucl. Phys. B **799** (2008) 34 [arXiv:0712.0481 [hep-ph]].
- [5] C. Peterson, D. Schlatter, I. Schmitt and P. M. Zerwas, Phys. Rev. D **27** (1983) 105.
- [6] B. A. Kniehl and G. Kramer, Phys. Rev. D **71** (2005) 094013 [hep-ph/0504058].
- [7] B. A. Kniehl and G. Kramer, Phys. Rev. D **74** (2006) 037502 [hep-ph/0607306].
- [8] G. Alexander *et al.* [OPAL Collaboration], Z. Phys. C **72** (1996) 1.
- [9] B. A. Kniehl, G. Kramer, I. Schienbein and H. Spiesberger, Eur. Phys. J. C **72** (2012) 2082 [arXiv:1202.0439 [hep-ph]].
- [10] R. Aaij *et al.* [LHCb Collaboration], Nucl. Phys. B **871** (2013) 1 [arXiv:1302.2864 [hep-ex]].
- [11] S. Acharya *et al.* [ALICE Collaboration], JHEP **1804** (2018) 108 [arXiv:1712.09581 [nucl-ex]].
- [12] A. M. Sirunyan *et al.* [CMS Collaboration], Phys. Lett. B **803** (2020) 135328 [arXiv:1906.03322 [hep-ex]].
- [13] M. Lisovskyi, A. Verbytskyi and O. Zenaiev, Eur. Phys. J. C **76** (2016) 397 [arXiv:1509.01061 [hep-ex]].
- [14] D. Bortoletto *et al.* [CLEO Collaboration], Phys. Rev. D **37** (1988) 1719 Erratum: [Phys. Rev. D **39** (1989) 1471].
- [15] P. Avery *et al.* [CLEO Collaboration], Phys. Rev. D **43** (1991) 3599.
- [16] H. Albrecht *et al.* [ARGUS Collaboration], Phys. Lett. B **207** (1988) 109.
- [17] B. Aubert *et al.* [BaBar Collaboration], Phys. Rev. D **75** (2007) 012003 [hep-ex/0609004].
- [18] G. Kramer and H. Spiesberger, Chin. Phys. C **42** (2018) 083102 [arXiv:1803.11103 [hep-ph]].

- [19] M. Niiyama *et al.* [Belle Collaboration], Phys. Rev. D **97** (2018) 072005 [arXiv:1706.06791 [hep-ex]].
- [20] B. A. Kniehl, G. Kramer, I. Schienbein and H. Spiesberger, Phys. Rev. D **71** (2005) 014018 [hep-ph/0410289].
- [21] B. A. Kniehl, G. Kramer, I. Schienbein and H. Spiesberger, Eur. Phys. J. C **41** (2005) 199 [hep-ph/0502194].
- [22] S. Dulat *et al.*, Phys. Rev. D **93** (2016) 033006 [arXiv:1506.07443 [hep-ph]].
- [23] A. Buckley, J. Ferrando, S. Lloyd, K. Nordström, B. Page, M. Rüfenacht, M. Schönherr and G. Watt, Eur. Phys. J. C **75** (2015) 132 [arXiv:1412.7420 [hep-ph]]. <http://projects.hepforge.org/hapdt/pdfsets>
- [24] M. Benzke, M. V. Garzelli, B. Kniehl, G. Kramer, S. Moch and G. Sigl, JHEP **1712** (2017) 021 [arXiv:1705.10386 [hep-ph]].
- [25] G. Kramer and H. Spiesberger, Phys. Rev. D **98** (2018) 114010 [arXiv:1809.04297 [hep-ph]].
- [26] S. Acharya *et al.* [ALICE Collaboration], Eur. Phys. J. C **77** (2017) 550 [arXiv:1702.00766 [hep-ex]].
- [27] J. Adam *et al.* [ALICE Collaboration], Phys. Rev. C **94** (2016) 054908 [arXiv:1605.07569 [nucl-ex]].
- [28] A. M. Sirunyan *et al.* [CMS Collaboration], Phys. Lett. B **782** (2018) 474 [arXiv:1708.04962 [nucl-ex]].
- [29] C. Patrignani *et al.* [Particle Data Group], Chin. Phys. C **40** (2016) 100001.
- [30] M. G. Bowler, Z. Phys. C **11** (1981) 169.
- [31] M. He and R. Rapp, Phys. Lett. B **795** (2019) 117 [arXiv:1902.08889 [nucl-th]].
- [32] J. R. Christiansen and P. Z. Skands, JHEP **1508** (2015) 003 [arXiv:1505.01681 [hep-ph]].
- [33] S. Shoeibi, F. Taghavi-Shahri, H. Khanpour and K. Javidan, Phys. Rev. D **97** (2018) 074013 [arXiv:1710.06329 [hep-ph]].
- [34] M. Salajegheh, S. M. Moosavi Nejad, M. Soleymaninia, H. Khanpour and S. Atashbar Tehrani, Eur. Phys. J. C **79** (2019) 999 [arXiv:1904.09832 [hep-ph]].
- [35] R. Maciula and A. Szczurek, Phys. Rev. D **98** (2018) 014016 [arXiv:1803.05807 [hep-ph]].